Diffusion kinetics of proton-induced ^{21}Ne, ^{3}He, and ^{4}He in quartz

DAVID L. SHUSTER* and KENNETH A. FARLEY

Division of Geological and Planetary Sciences, MC 100-23, California Institute of Technology, Pasadena, CA 91125, USA

Abstract—A natural quartz sample free of mineral and fluid inclusions was irradiated with a 200 MeV proton beam to produce spallogenic ^{21}Ne, ^{3}He and ^{4}He. Temperature-dependent diffusivities of these three nuclides were then determined simultaneously by high precision stepped-heating and noble gas mass spectrometry. The outward mobility of proton-induced nuclides reflects diffusion through the quartz lattice. In the studied range of 70 to 400°C the helium diffusion coefficients exceed those of neon by 5–7 orders of magnitude. The implied diffusion parameters $E_a = 153.7 \pm 1.5$ (kJ/mol) and $\ln(D_o/a^2) = 15.9 \pm 0.3$ (ln(s^{-1})) and $E_a = 84.5 \pm 1.2$ (kJ/mol) and $\ln(D_o/a^2) = 11.1 \pm 0.3$ (ln(s^{-1})) for proton-induced ^{21}Ne and ^{3}He, respectively, indicate that cosmogenic neon will be quantitatively retained in inclusion-free quartz at typical Earth surface temperatures whereas cosmogenic helium will not. However, the neon diffusion parameters also indicate that diffusive loss needs to be considered for small (<1 mm) quartz grains that have experienced elevated temperatures. Since natural quartz often contains fluid inclusions which may enhance noble gas retentivity, these parameters likely represent an end-member case of purely solid-state diffusion. The ~70 kJ/mol higher activation energy for neon diffusion compared to helium diffusion likely represents an energy barrier related to its ~13% greater diameter and provides a fundamental constraint with which to test theories of solid state diffusion. The diffusion parameters for proton-induced ^{4}He are indistinguishable from those for ^{3}He, providing no evidence for the commonly expected inverse square root of the mass diffusion relationship between isotopes. We also find preliminary indication that increased exposure to radiation may enhance neon and helium retentivity in quartz at low temperatures. *Copyright © 2005 Elsevier Ltd*

1. INTRODUCTION

Over the last two decades, measurement of the stable cosmogenic noble gases ^{3}He, ^{4}He, ^{21}Ne, ^{22}Ne, ^{38}Ar and ^{83}Kr has become an essential tool for determining the exposure duration of terrestrial and extraterrestrial materials to cosmic rays (Niedermann, 2002; Wieler, 2002). With knowledge of the production rate and the retentivity of a cosmogenic nuclide in a specific mineral, a surface exposure timescale can be calculated from an atomic concentration in that mineral. For example, cosmogenic ^{21}Ne concentrations in quartz are widely used to constrain erosion rates or exposure ages in terrestrial geological problems (Lal, 1988; Cerling and Craig, 1993; Niedermann et al., 1993; Cerling et al., 1994; Bruno et al., 1997; Phillips et al., 1998; Hetzel et al., 2002; Libarkin et al., 2002; Niedermann, 2002). Although much work has been done to calibrate and understand the terrestrial production rate of helium and neon in quartz (Masarik et al., 2001a; Niedermann, 2002), their diffusion kinetics in this mineral have not been well characterized. The general consistency between ^{21}Ne-based exposure ages and those based on ^{10}Be and ^{26}Al concentrations has been used to argue for quantitative retention of ^{21}Ne in quartz under Earth surface conditions (Bruno et al., 1997; Schafer et al., 1999; Hetzel et al., 2002) but provides no information on the temperature dependence of diffusivity nor insight to whether small quartz grains might incompletely retain neon. In the case of helium, the experimental results of Trull et al. (1991) suggest nearly quantitative retention over 10^6 yr timescales in quartz, but exposure ages of natural quartz samples indicate otherwise

(Brook and Kurz, 1993; Trull et al., 1995; Niedermann, 2002). The inconsistency between exposure ages derived from ^{3}He and those based on ^{10}Be and ^{26}Al has been interpreted to indicate that quartz does not retain helium at typical Earth surface temperatures. A successful physical model of solid state diffusion should be able to predict why quartz should apparently retain neon but not retain helium.

The current mechanistic understanding of solid state diffusion of noble gases through crystalline materials is based on limited experimental results. Measurement of diffusion coefficients typically entails the direct determination of concentration profiles following inward diffusion (charging experiments, e.g., Watson and Cherniak, 2003) or, more commonly, measuring gas release during step-heating of a sample with either natural or artificially added diffusant (degassing experiments, e.g., Fechtig and Kalbitzer, 1966; Dunai and Roselieb, 1996; Farley, 2000; Shuster et al., 2004). Owing to analytical challenges of directly measuring noble gas concentration profiles over small length-scales (<1 μm), the latter is usually more straightforward and precise. Calculating diffusion coefficients from a degassing experiment requires specification of the initial spatial distribution of the diffusant. Because spatial distributions of naturally occurring noble gases are commonly unknown, the results can be uncertain and will be erroneous if the actual distribution is not equivalent to the assumed initial distribution (Shuster and Farley, 2004). Furthermore, since the activation energy of a migrating noble gas atom may depend on the specific siting that the atom initially occupies in a mineral matrix, degassing experiments can be complicated by the presence of multiple noble gas components as well as radiation damage and fluid and mineral inclusions (Crank, 1975; Trull et al., 1991; Niedermann et al., 1993; Farley, 2000).

---

* Author to whom correspondence should be addressed (dshuster@caltech.edu).

D. L. Shuster and K. A. Farley

Table 1. Dose/yield summary for quartz[a]

Experiment	Fluence ($\times 10^{15}$ p/cm^2)	Proton energy (MeV)	[^{21}Ne] (atoms/mg)	^{22}Ne/^{21}Ne	[^{3}He] (atoms/mg)	^{4}He/^{3}He
	0	n.a.	$<5.00 \times 10^4$	$\sim 10^1$	$<1.00 \times 10^3$	$\sim 10^4$
1	6.3	200	6.61×10^8	0.61	1.57×10^9	10.31
2 (lower dose)	0.2	150	0.31×10^8	0.78	0.04×10^9	—

[a] The proton fluences and energies were estimated by each aliquot's position within the target stacks as discussed in (Shuster et al., 2004). Uncertainty in the dose and energy is estimated to be ±10% relative error. For the irradiated samples, we estimate the atomic concentrations to be better than ±5% for each presented nuclide. The concentrations for zero fluence are the natural concentrations determined on an unirradiated aliquot. Note that ^{21}Ne and ^{3}He (and ^{4}He in Experiment 1) in the irradiated samples are almost exclusively synthetic. Measurements of Experiment 1 were made 12 months after irradiation, and those of Experiment 2 were made 24 months after irradiation. n.a. = applicable; dash = below detection limit.

Here we present the results of two experiments in which the diffusion kinetics of proton-induced ^{21}Ne and ^{3}He (and ^{4}He in one experiment) were determined in a natural sample of quartz using the step-heating technique. The first experiment used higher proton fluence (see Methods), and an additional experiment used a proton fluence ~one order of magnitude lower to test for possible effects that proton irradiation may have upon diffusion kinetics. By irradiating quartz with a 150–200 MeV proton beam, we induced nuclear transmutations of the Si and O atoms to generate a uniform distribution of purely synthetic, single component noble gases. The ability to generate multiple elements and isotopes makes proton-induced noble gases attractive for studying size and isotope effects in solid state diffusion.

Because the nuclear transmutations in our experiments are similar to those which occur through cosmic ray interactions in quartz, the proton-induced nuclides should be good analogs for naturally occurring cosmogenic neon and helium (see Discussion). Moderate and high-energy proton bombardment produces spallation ^{3}He from both Si and O in exactly the same way that cosmogenic ^{3}He is produced in meteorites in space (Leya et al., 1998; Wieler, 2002; Shuster et al., 2004). Since Si nuclei are effectively the only targets which produce ^{21}Ne in our sample, a relatively limited number of multiple stage production pathways are probable and should also be the same as those which occur in nature.

2. SAMPLE DESCRIPTION AND METHODS

The analyzed sample was pure quartz collected from a quartz vein in Conselheiro Mata, Minas Gerais, Brazil (GRR-1668). The specimen was a gem quality, optically clear single prismatic crystal of approximate dimensions $9 \times 0.5 \times 0.5$ cm and was microscopically inspected to be free of mineral and fluid inclusions. Shown in Table 1 are the natural concentrations of ^{21}Ne, ^{3}He and ^{4}He in an aliquot of this sample, which indicate that it was essentially free of these nuclides before proton irradiation. We separately irradiated two ~100 mg shards broken from the specimen's interior.

Details of the proton irradiations and analytical procedures have been described elsewhere (Shuster et al., 2004). In the first experiment (experiment 1), the quartz sample was placed in an aluminum container and exposed to a 200 MeV proton beam for a continuous 8 h period at the Northeast Proton Therapy Center receiving a fluence of ~6.3 $\times 10^{15}$ protons/cm^2. We estimate that the analyzed aliquot received a total dose of ~3.7 $\times 10^{13}$ protons. The sample temperature did not exceed 45°C during proton bombardment.

The diffusion experiment was performed ~12 months after the proton irradiation. To ensure that each nuclide had an initially uniform distribution, a ~430 μm (radius) aliquot was broken out of the interior of the original ~2 mm shard just before analysis. By analyzing an interior portion of the sample, we minimized the potential that the neon

and helium distributions in the analyzed aliquot had become diffusively modified between irradiation and analysis.

The second experiment (experiment 2, lower proton dose) was performed on an aliquot of the same sample and used the same procedures as described above. However, the aliquot was irradiated with a ~150 MeV proton beam and received a total fluence of only ~2 $\times 10^{14}$ p/cm^2. This irradiation took place ~24 months before the step-heating analysis.

The aliquots were each held at a known temperature for a known time in a volume of ~300 cm^3 under static vacuum (Farley et al., 1999). We then measured the isotopic abundances of helium and neon at each heating step to determine diffusion coefficients. Helium and neon were cryogenically separated using activated charcoal; each element was analyzed separately on a MAP 215-50 mass spectrometer. We converted measured release fractions and the duration of each step to diffusion coefficients using published equations (Fechtig and Kalbitzer, 1966) and the assumptions therein. The estimated uncertainty on temperatures was better than ±2°C and on diffusion coefficients better than ±0.2 natural log units for all points used in the regressions. From calculated diffusion coefficients and the temperature of each step, we generated Arrhenius plots to determine the activation energy, E_a, and frequency factor, D_o/a^2 by linear regression to define the function $D(T)/a^2 = D_o/a^2 \exp(-E_a/RT)$ (D is the diffusion coefficient, a is the characteristic length scale of the analyzed diffusion domain, R is the gas constant). We assumed spherical geometry and initially uniform concentration profiles for each nuclide. To verify the assumed initial conditions of the experiment, the heating schedules included isothermal steps as well as both prograde and retrograde heating cycles (see Tables 2 and 4) (Shuster and Farley, 2004).

3. RESULTS

The total concentrations of proton-induced ^{21}Ne, ^{3}He and ^{4}He are summarized in Table 1. These concentrations are generally higher than the wide range of natural cosmogenic concentrations that have been observed in quartz. Cosmogenic ^{21}Ne concentrations in terrestrial quartz are of order 10^6–10^8 atoms/g (Graf et al., 1991; Niedermann et al., 1993; Cerling et al., 1994; Hetzel et al., 2002; Libarkin et al., 2002; Niedermann, 2002) and in meteorites they are more variable and generally larger, 10^7–10^{10} atoms/g (Masarik et al., 2001b; Wieler, 2002). Observations of cosmogenic ^{3}He concentrations in terrestrial quartz are more sparse, but of order 10^6–10^8 atoms/g (Trull et al., 1991; Brook and Kurz, 1993).

The results of diffusion experiment 1 for each isotope are presented in Table 2, and shown in Figure 1 as a single Arrhenius plot. Regression statistics and the diffusion parameters D_o/a^2 and E_a are summarized for each isotope in Table 2. We find that the calculated neon diffusion coefficients (D/a^2) are 5–7 orders of magnitude lower than the helium coefficients for temperatures at which both values were determined (between 100°C and 250°C). The Arrhenius plots show strong

Table 2. Stepped heating results (Experiment 1).[a]

Step	T (°C)	t (hr)	3He (×10⁶ atoms)	±	4He/3He	±	21Ne (×10⁶ atoms)	±
1	99.5	0.5	48.3	0.9	8.5	1.7	—	—
2	99.8	1.0	50.0	1.0	9.2	1.7	—	—
3	99.8	2.0	67.1	0.8	12.9	1.2	—	—
4	79.9	1.0	7.1	0.4	10.4	3.7	—	—
5	79.9	1.0	6.8	0.4	10.3	3.7	—	—
6	70.0	2.0	5.7	0.2	10.5	2.9	—	—
7	69.9	2.0	5.3	0.4	10.5	3.3	—	—
8	69.8	2.0	4.6	0.1	10.5	3.3	—	—
9	89.8	1.5	17.3	0.7	12.0	1.9	—	—
10	89.8	2.0	23.1	0.7	12.0	1.6	—	—
11	99.8	1.5	33.5	1.0	10.8	1.2	—	—
12	119.5	0.5	42.3	0.9	9.7	0.9	—	—
13	119.6	0.5	38.0	1.0	9.6	1.0	—	—
14	119.2	0.5	33.4	0.8	10.5	1.1	0.05	0.10
15	139.4	0.5	101.2	1.5	10.0	0.4	0.04	0.09
16	139.4	0.5	75.0	1.6	9.9	0.6	0.03	0.10
17	139.7	1.0	114.6	1.8	10.3	0.4	0.04	0.07
18	159.2	0.5	139.1	2.3	10.3	0.3	0.08	0.05
19	159.9	1.0	186.8	2.4	10.2	0.2	0.12	0.05
20	174.2	0.5	157.7	2.0	10.1	0.3	0.16	0.05
21	174.6	0.5	111.2	1.7	10.1	0.4	0.11	0.05
22	199.7	1.0	321.2	3.0	10.3	0.1	0.84	0.09
23	199.9	0.5	59.6	1.1	10.1	0.7	0.25	0.05
24	224.8	0.5	73.6	1.2	10.4	0.6	1.16	0.10
25	224.9	1.0	23.1	1.3	12.6	1.6	1.29	0.13
26	249.8	0.5	2.0	0.8	9.0	2.3	2.65	0.16
27	249.8	1.0	—	—	—	—	3.49	0.21
28	274.8	0.5	—	—	—	—	6.26	0.24
29	275.0	1.0	—	—	—	—	8.91	0.29
30	299.8	0.5	—	—	—	—	15.36	0.32
31	299.7	1.0	—	—	—	—	20.13	0.47
32	324.9	0.5	—	—	—	—	29.20	0.57
33	324.8	1.0	—	—	—	—	38.52	0.72
34	350.1	0.5	—	—	—	—	46.25	0.66
35	349.7	1.0	—	—	—	—	55.01	0.78
36	337.7	1.0	—	—	—	—	21.31	0.58
37	311.7	1.3	—	—	—	—	5.88	0.24
38	287.8	1.5	—	—	—	—	1.76	0.11
39	259.3	2.0	—	—	—	—	0.42	0.07
40	238.0	3.0	—	—	—	—	0.14	0.05
41	250.0	2.0	—	—	—	—	0.19	0.06
42	274.9	1.5	—	—	—	—	0.70	0.08
43	299.9	1.0	—	—	—	—	2.41	0.18
44	324.8	0.5	—	—	—	—	4.99	0.22
45	349.9	1.0	—	—	—	—	30.38	0.51
46	374.9	1.0	—	—	—	—	64.97	0.80
47	399.9	1.0	—	—	—	—	98.85	1.00
Fusion	~1300	0.5	—	—	—	—	272.40	2.15
Total			1747.6				734.34	

[a] All values are corrected for blank contributions. A dash indicates below detection limit. Mass analyzed = 1.11 mg.

linear correlations between ln(D/a²) and 1/T and reveal distinct diffusion parameters for each element.

The linear correlation between the 21Ne diffusion coefficients and 1/T persists throughout the entire experiment, including a retrograde cycle and multiple isothermal steps between 125°C and 400°C. From linear regression, the 21Ne diffusion parameters are: E_a = 153.7 ± 1.5 (kJ/mol) and $\ln(D_o/a^2)$ = 15.9 ± 0.3 ($\ln(s^{-1})$) (SE; n = 30).

Diffusion coefficients for the two helium isotopes are indistinguishable from each other as shown in Figure 1. Indeed, the diffusion coefficients for both isotopes plot on top of one another at each temperature. With the exception of the first three measurements (at 100°C, initial ~8% of the total gas yield), the diffusion coefficients plot on a line. For the first three points we observe a small and progressively decreasing deficit in the 3He and 4He diffusion coefficients (maximum deficit of ~1 ln unit; see Fig. 1), where we define deficit to be anomalously low diffusion coefficients with respect to the array defined by the bulk of the data. The slight deficit may be related to the diffusive rounding of the helium isotope distributions during the 12 months spent at room temperature between proton irradiation and the degassing experiment (see Discussion). Although we broke out an interior aliquot, it is possible that we did not completely avoid portions of the sample that had been diffusively modified. We therefore excluded these steps from Arrhenius regressions. Following these initial steps,
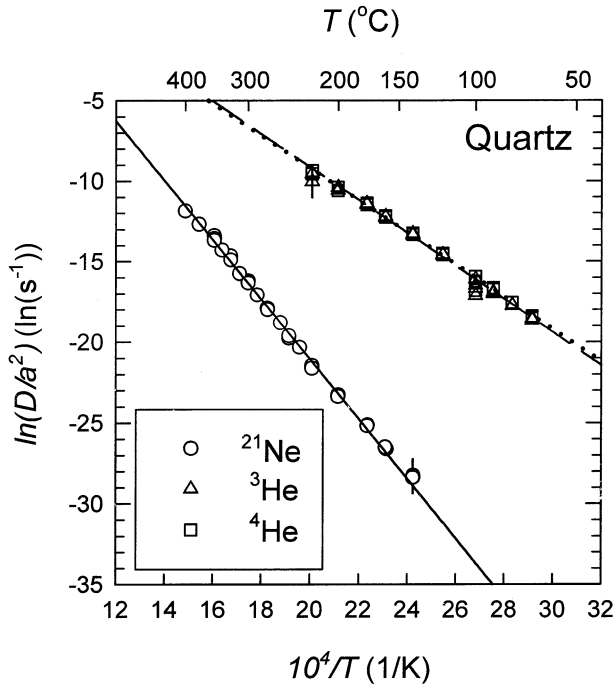
Fig. 1. Arrhenius plot for proton-induced nuclides (Experiment 1). Open circles are values calculated from ^{21}Ne, triangles from ^{3}He and squares from ^{4}He results shown in Table 2. Solid line indicates least squares regression through the ^{21}Ne results; dashed and dotted line through a subset of the ^{3}He and ^{4}He results, respectively.

Fig. 2. Ratio evolution diagram (Experiment 1). Shown are measured helium isotope ratios for each release step, ^{4}He/^{3}He$_{step}$, plotted vs. the cumulative ^{3}He release fraction, ΣF^{3}He. Four diffusion models are shown. The model of equivalent diffusivity, D^{4}He/D^{3}He $= 1.00$, which well fits the entire data set, is shown as a solid gray line. Of particular significance are the 12 points plotting between $0.30 < \Sigma F^{3}$He < 0.99. Two reference models are shown as solid black curves: D^{4}He/D^{3}He $= \sqrt{m_3 m_4} = 0.868$. The magnitude of the error bars are dominated by and estimated by uncertainty in the ^{4}He blank corrections. The inset shows the error-weighted residual sums of squares between models calculated for a given value of D^{4}He/D^{3}He and the entire set of ^{4}He/^{3}He observations.

strong linear correlation persists throughout a retrograde temperature cycle and multiple isothermal steps between 70°C and 200°C. Over these steps, ~90% of the helium was evolved from the sample. These data imply $E_a = 84.5 \pm 1.2$ (kJ/mol) and $\ln(D_o/a^2) = 11.1 \pm 0.3$ (ln(s^{-1})) (SE; $n = 21$) and $E_a = 83.2 \pm 0.8$ (kJ/mol) and $\ln(D_o/a^2) = 10.8 \pm 0.3$ (ln(s^{-1})) (SE; $n = 21$) for ^{3}He and ^{4}He, respectively.

To highlight similarity in the diffusivity of the two helium isotopes, we also present in Figure 2 the degassing results as a ratio evolution diagram (^{4}He/^{3}He$_{step}$ vs. ΣF^{3}He where ^{4}He/^{3}He$_{step}$ is the measured ratio at each step, and ΣF^{3}He is the cumulative ^{3}He release fraction; Shuster and Farley, 2004; Shuster et al., 2004). Diffusivity ratios D^{4}He/D^{3}He other than unity will cause values of ^{4}He/^{3}He$_{step}$ to systematically deviate from the bulk ratio at high values of ΣF^{3}He. Throughout the entire experiment the observed ^{4}He/^{3}He ratios are very nearly constant indicating nearly identical diffusivities. Although there is scatter in the initial steps (predominantly due to the magnitude and uncertainty in ^{4}He blank corrections at those steps), we find no significant deviation from the bulk ^{4}He/^{3}He ratio when $0.20 < \Sigma F_i^{3H3} < 0.99$. Shown in the inset of Figure 2 are the error weighted residual sums of squares between models calculated for a given value of D^{4}He/D^{3}He and our ^{4}He/^{3}He observations. For models of nearly equivalent diffusivity (i.e., D^{4}He/D^{3}He $= 1$ and 1.05), we find residual sums of squares that are approximately two orders of magnitude smaller than that for the canonical inverse root mass relationship, indicating that these models more successfully predict the data. In the discussion below, we will focus on ^{3}He rather than ^{4}He
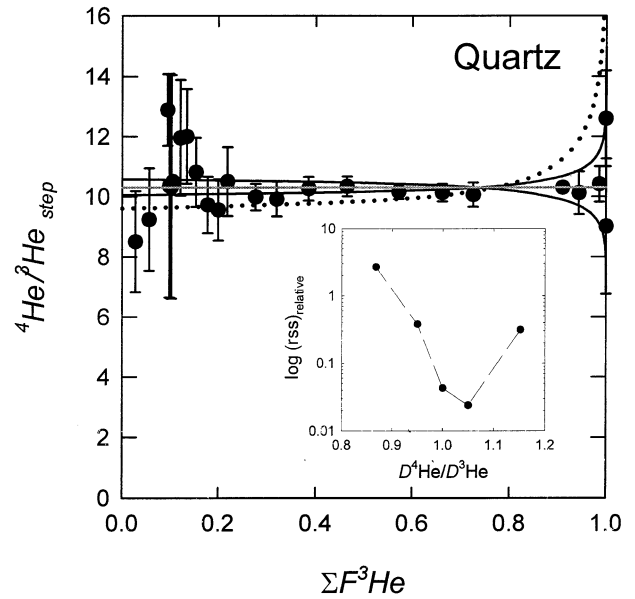
diffusivity because the ^{3}He results have better analytical precision.

The results of diffusion experiment 2 (lower proton dose) for each isotope are presented in Table 4, and shown in Figure 3 as an Arrhenius plot. These results are presented and discussed in more detail below (see section 4.3).

4. DISCUSSION

4.1. Diffusion Kinetics of Proton-Induced Nuclides

We believe the diffusion parameters of proton-induced ^{21}Ne, ^{3}He and ^{4}He are well characterized by experiment 1 for a number of reasons. The persistence of Arrhenian linearity throughout retrograde heating cycles and isothermal heating steps precludes the possibility of several complications. Retrograde temperature cycling is sensitive to (i) the presence of an initial distribution that is not uniform and (ii) the presence of a distribution of domain sizes (Lovera et al., 1989; McDougall and Harrison, 1999; Shuster et al., 2005). Under the conditions of the experiment, both complications would result in nonlinear patterns which are not observed in Figure 1. Furthermore, since the experiment was conducted at low temperatures, and since the correlations persist over significant cumulative fractions for each gas, we can rule out the presence of inclusions with distinct retention properties. Each of these complications is
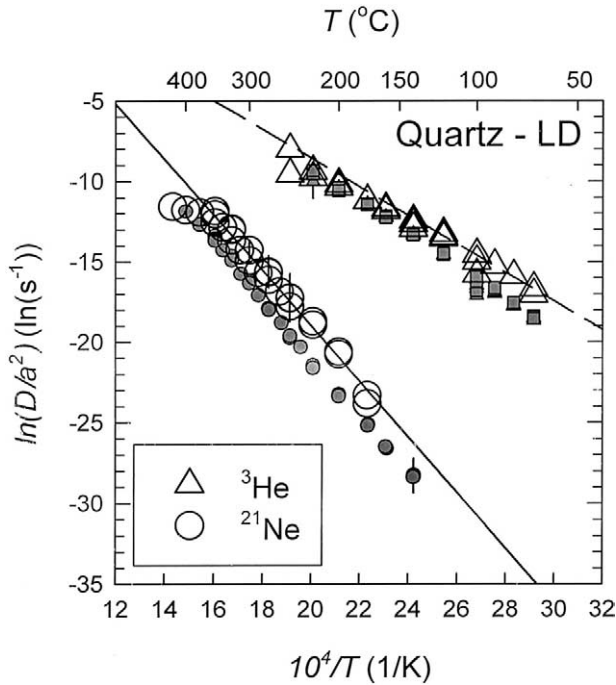
Fig. 3. Arrhenius plot for proton-induced nuclides (Experiment 2, lower proton dose). Open points are results of ~0.03 times the dose shown in Figure 1. Open circles are values calculated from ^{21}Ne, triangles from ^{3}He results shown in Table 4. Also shown for reference as solid points are the same results shown in Figure 1. The solid line indicates least squares regression through a subset of the ^{21}Ne results, dashed line through a subset of the ^{3}He results of Experiment 2.

usually expressed in an Arrhenius plot as a "break in slope," which is clearly not observed in Figure 1.

The room temperature diffusivity of proton-induced helium is sufficiently high to have caused diffusive loss from the irradiated sample over month timescales. For instance, we estimate that the original 2 mm (radius) grain would have lost ~5% of its helium between the time of irradiation and analysis, causing a diffusively rounded profile in the outer ~50 μm. It was critical for our experiment that we broke out an interior aliquot for the analysis, yet we still apparently observe the effect of diffusive rounding. The influence of even ~1% loss could result in the slight deficit observed in Figure 1 (Shuster and Farley, 2004). Note than diffusive loss of ^{21}Ne over this time would be negligible.

4.2. Proton-Induced Nuclides as Cosmogenic Analogs

An important question for interpreting and comparing our diffusion parameters with those determined for naturally occurring cosmogenic nuclides is whether the synthetically and naturally produced nuclides are analogous. If the proton-induced nuclides are produced through significantly different production pathways and with different energies than in nature, their initial siting in the quartz lattice could be different. Although not at all clear what influence the initial siting should have upon noble gas diffusion kinetics in quartz, these possibilities require consideration.

Silicon is transmuted to neon and helium through multistage production pathways. These pathways likely involve the "evaporation" of charged particles from an excited residual nucleus (Friedlander et al., 1981; Shuster et al., 2004). In spallation reactions involving charged particle evaporation, the kinetic energies of the "evaporation" particles (e.g., ^{3}He, ^{4}He, p, n, etc.) and residual nuclei (e.g., ^{21}Ne) are not expected to be a function of incident particle energy above a certain threshold. Therefore, the kinetic energies of the final spallation products induced by 200 MeV protons are likely to be similar to those produced in situ from primary galactic cosmic ray protons which have peak energy of ~650 MeV (Leya et al., 2000). Cosmogenic and proton-induced ^{21}Ne are not expected to have energies greater than 1 MeV/amu; the ^{21}Ne nuclei are likely to have traversed at least several tens of lattice spaces from the original Si siting. The ejection trajectories of the charged particles should be approximately stochastic so the final ^{21}Ne distribution is expected to be very nearly uniform throughout the crystal. Since the production ratio of ^{22}Ne/^{21}Ne is somewhat dependent upon the energy of the incident particle(s) (Leya et al., 1998), a comparison between the ^{22}Ne/^{21}Ne ratio induced in our sample and natural cosmogenic ^{22}Ne/^{21}Ne ratios should provide some insight to the respective production mechanisms.

Leya et al. (1998) measured cross sections for the reactions Si(p,X)^{21}Ne and Si(p,X)^{22}Ne with 180 MeV protons: $\sigma_d(^{21}$Ne$)$ = 18.5 ± 1.0 mb, $\sigma_d(^{22}$Ne$)$ = 7.6 ± 0.9 mb, and $\sigma_c(^{22}$Ne$)$ = 24.9 ± 3.3 mb, where X represents the cumulative spallation products complementary to ^{21}Ne or ^{22}Ne, σ_d is the cross section calculated for instantaneous production, and σ_c is the cumulative cross section which takes into account delayed production from the decay of proton-induced ^{22}Na (mean life τ = 3.76 yr). From these data, we expect an instantaneous ^{22}Ne/^{21}Ne production ratio of 0.41 ± 0.05, and a gradual increase in the ^{22}Ne/^{21}Ne over time to a value of ~1.3 ± 0.2 as ^{22}Na decays. If we estimate an initial ^{22}Na/^{21}Ne production ratio of 0.89 (Leya et al., 1998), then after 1 yr we expect to have a ^{22}Ne/^{21}Ne ratio of ~0.62. This is in excellent agreement with the ^{22}Ne/^{21}Ne ratio in our sample, 0.61, implying that the cumulative ^{22}Ne/^{21}Ne ratio produced in our sample will become ~1.3 after ^{22}Na has completely decayed.

Leya et al. (1998) also measured cross sections for the reactions Si(p,X)^{4}He and Si(p,X)^{3}He with 180 MeV protons: $\sigma_d(^{3}$He$)$ = 18.3 ± 1.1 mb, $\sigma_c(^{4}$He$)$ = 202 ± 11 mb. From these data, we expect an instantaneous ^{4}He/^{3}He production ratio of ~11. If we assume a ^{3}H/^{3}He production ratio of 1 (Leya et al., 1998), then after 1 yr, we expect a ^{4}He/^{3}He ratio of 10.4, which is also in excellent agreement with the observed ratio in our sample of ~10.3.

Several studies have constrained the natural cosmogenic ^{22}Ne/^{21}Ne production ratio in extraterrestrial (1.05 to 1.25; Leya et al., 2000; Masarik et al., 2001b) and terrestrial samples (1.22–1.27; Niedermann et al., 1993; Bruno et al., 1997; Phillips et al., 1998). Because the implied cumulative ^{22}Ne/^{21}Ne ratio in our sample (~1.3 ± 0.2) is in excellent agreement with natural cosmogenic ratios, we believe that the proton-induced neon in our experiment is a good analog for a purely cosmogenic component of neon. And, since the production cross sections and ^{22}Ne/^{21}Ne production ratios remain roughly constant above an apparent proton energy threshold of ~80 MeV (Leya et al., 1998), the final energies and hence final production

mechanisms of the synthetically produced and natural cosmogenic ^{21}Ne nuclei are not likely to be significantly different.

4.3. Does Proton Irradiation Affect Noble Gas Diffusion Kinetics in Quartz?

Previous efforts to quantify noble gas diffusivities following proton or neutron irradiation have emphasized a need to evaluate the possibility that irradiation induced lattice damage modifies what would otherwise be a material's natural diffusion kinetics (Luther and Moore, 1964; Horn et al., 1975; Wiens et al., 1994; Onstott et al., 1995; Shuster et al., 2004). Unlike neutrons, accelerated protons primarily lose energy by electronic stopping: ionizing collisions with electrons resulting in no lattice damage. For equivalent nucleon fluence, protons are expected to result in significantly less lattice damage than neutrons. Shuster et al. (2004) unambiguously demonstrated that proton irradiation causes no detectable modification of natural ^{4}He diffusion kinetics in apatite and titanite when using a proton energy of ~150 MeV and a fluence of 2 to 5 × 10^{14} p/cm^2.

The results of Shuster et al. (2004) cannot be simply extrapolated from apatite and titanite to quartz for a number of reasons. Since the energies associated with specific nuclear transmutations will depend on target chemistry, the induced damage to a mineral lattice may vary from mineral to mineral. Furthermore, the U and Th bearing minerals studied by Shuster et al. (2004) contained significant natural radiation damage associated with spontaneous fission, alpha tracks, and alpha recoil. If radiation damage somehow influences the noble gas diffusion kinetics in a particular material, then the additional damage induced by proton irradiation may introduce a negligible net effect. On the other hand, because the quartz sample of the present study did not possess significant natural radiation damage, the possibility remains that the proton-induced damage could have modified diffusivity.

To assess this issue, we performed an additional experiment (experiment 2) on the same quartz sample, but using a 2.80 mg aliquot which was irradiated to a much lower proton dose. The irradiation was performed nearly 2 yr before the diffusion experiment with a proton energy of ~150 MeV and a total fluence of ~2 × 10^{14} p/cm^2. With exception to the dose, the methods used were the same as in experiment 1. Due to the lower proton fluence, the total ^{21}Ne and ^{3}He concentrations were lower than in experiment 1 by factors of ~0.05 and ~0.03, respectively. This resulted in significantly larger blank corrections on many heating steps and greater scatter in the overall results. All ^{4}He measurements were below the detection limit, so ^{4}He/^{3}He ratios were not determined. Despite these complications, we were able to reasonably constrain the diffusion kinetics of ^{21}Ne and ^{3}He in the aliquot.

The results of the "low dose" diffusion experiment for each isotope are presented in Table 4, and shown in Figure 3 as an Arrhenius plot. As with the primary experiment, we find calculated ^{21}Ne diffusion coefficients (D/a^2) that are 5–7 orders of magnitude lower than the ^{3}He coefficients for temperatures at which both values were determined (between 100°C and 250°C). The Arrhenius plots show strong linear correlations between ln(D/a^2) and 1/T and reveal distinct diffusion parameters for each element. Although qualitatively consistent with

Figure 1, the results indicate slightly different diffusion parameters with a rotation of the arrays toward slightly higher diffusivities at low temperatures. We also observe slight curvature in the ^{21}Ne results above ~400°C and in the ^{3}He results above ~150°C. Regressions through the linear subsets of the data (i.e., excluding apparent curvature) indicate the following parameters: E$_a$ = 143 ± 4 (kJ/mol) and ln(D$_o$/a^2) = 15.5 ± 1 (ln(s^{-1})) (SE; n = 21) and E$_a$ = 74 ± 3 (kJ/mol) and ln(D$_o$/a^2) = 9 ± 1 (ln(s^{-1})) (SE; n = 10) for ^{21}Ne and ^{3}He, respectively, and are shown in Figure 3. The difference in activation energy is 69 (kJ/mol), which is in excellent agreement with the high dose result (Fig. 1).

Although the results of the two experiments are in good agreement with one another, each indicates statistically distinct diffusion parameters. And although the discrepancy may relate to unidentified heterogeneity between the aliquots, we cannot rule out the possibility that the accumulation of radiation damage may have a small effect on neon and helium diffusion in quartz. Figure 3 suggests that an increase in radiation exposure causes quartz to become more retentive of both elements at low temperatures. If radiation induces a significant number of dislocations which increase the abundance of isolated "void spaces," the damage may introduce the same effect as micro- or nanofluid inclusions, which would increase overall noble gas retentivity in a solid material. This implies that natural quartz with typical cosmic ray exposure would have less radiation damage than in our experiments and therefore may be less retentive than our results indicate. Additional controlled experiments are required to more fully assess this hypothesis and to quantify the magnitude of the potential effect which may also occur in nature. Since the slight discrepancy between the two results does not influence our major conclusions, we focus our discussion on the better-constrained experimental results at higher proton fluence and the implications of the parameters summarized in Table 3.

4.4. Diffusion Results in the Context of Previous Studies

Although not their primary objective, Niedermann et al. (1993) estimated neon diffusion kinetics in quartz. They were able to constrain the activation energy for natural cosmogenic ^{21}Ne diffusion by de-convolving the cosmogenic and trapped atmospheric components at each of their degassing steps. Given the complication of two component de-convolution and the coarseness of their Arrhenius regression (n = 4), it is unclear whether the discrepancy between the value they obtained (E$_a$ = 90 ± 10 kJ/mol) and the one obtained in the present study is significant.

Four previous studies have reported helium diffusivities in quartz (Funk et al., 1971; Trull et al., 1991; Brook and Kurz, 1993; Argunova et al., 2003). Of these, only those of Funk et al. (1971) and Trull et al. (1991) quantified the temperature dependence. Funk et al. (1971) constrained only the activation energy in quartz to be 54–67 (kJ/mol). Trull et al. (1991) found E$_a$ = 106 ± 4 (kJ/mol) and ln(D$_o$) = 0.5 ± 0.9 (ln(s^{-1})), by degassing natural cosmogenic ^{3}He from an Antarctic quartz sample. These activation energies are directly comparable with our results, but to compare the frequency factors we must assume that the bulk geometries of the analyzed grains define the diffusion domain in each experiment. Although the differ-

Table 3. Diffusion coefficient summary (Experiment 1).[a]

Nuclide	R^2	d.f.	$\ln(D_o/a^2)$ $(\ln(s^{-1}))$	±	E_a (kJ/mol)	±
^{21}Ne	0.997	29	15.9	0.3	153.7	1.5
^{3}He	0.997	20	11.1	0.3	84.5	1.2
^{4}He	0.998	20	10.8	0.3	83.2	0.8

[a] Standard errors in the regression statistics are reported at the 95% confidence level. d.f. = degrees of freedom in regression.

ence in activation energy between our finding and that of Trull et al. (1991) is statistically significant, it is relatively small (21%) when compared to the difference of ~5 orders of magnitude in the frequency factors. After normalizing each result for their difference in grain size and extrapolating to 20°C, our results predict a helium diffusion coefficient that is ~6 orders of magnitude higher than that predicted by Trull et al. (1991). The result of Trull et al. (1991) predicts diffusive helium loss fractions of order % from 2 mm quartz grains held at 20°C over ~Myr timescales, whereas our result predicts effectively no retention.

The diffusion parameters reported by Trull et al. (1991) are based on many data points that form a linear Arrhenius array, yet they are very different form our measurements. This discrepancy requires explanation. As noted above, previous attempts to measure cosmogenic exposure ages using ^{3}He in quartz have suggested that helium leaks at earth surface temperatures, despite the high degree of retentivity implied by the Trull et al. (1991) parameters. This suggests variability in He diffusion parameters from sample to sample.

The quartz specimen that Trull et al. (1991) studied contained visible inclusions of 5–15 μm in size; the magnitude of the effects that mineral inclusions, fluid inclusions, radiation damage and defect density have upon solid state diffusion remains poorly understood. If helium diffusivity in quartz somehow depends on the presence and volume densities of these features, then they need to be considered when generalizing experimentally determined parameters to other samples.

By measuring the bulk ^{3}He concentrations in different size fractions, Brook and Kurz (1993) concluded that greater diffusive loss had occurred in smaller quartz grains than in larger grains. They used their data to coarsely estimate a helium diffusion coefficient of $1.5–5 \times 10^{-18}$ cm^2/s, which is 2 orders of magnitude higher than that predicted by Trull et al. (1991) but 3 orders of magnitude lower than our results when extrapolated to 0°C. Like Trull et al. (1991), Brook and Kurz (1993) also observed a clear cosmogenic signature (high ^{3}He/^{4}He) and high helium concentrations in the fluid inclusions of their quartz samples.

Although our results are qualitatively consistent with empiric arguments that quartz incompletely retains helium over geologic time, the diffusion parameters in Table 2 predict even less retention than that which has been observed (Trull et al., 1991; Brook and Kurz, 1993). We suggest that the observed variability between these studies is due to the presence or absence of (micro) fluid inclusions. Strong partitioning of helium into fluid inclusions and potentially into sites of radiation damage may cause diffusivity to be slower than solid state diffusion parameters would otherwise predict (Crank, 1975; Trull et al., 1991;

Farley, 2000). For instance, the quartz specimen used here was specifically selected for the absence of fluid inclusions whereas the previously studied samples had inclusions clearly containing ^{3}He. By melting whole grains containing inclusions, the ^{3}He diffusivity estimated by Brook and Kurz (1993) is an effective parameter convolving both the solid state diffusivity and the fluid/solid partitioning function of their sample. Trull et al. (1991) also called upon the effect of partitioning to explain why they observed radiogenic ^{4}He diffusion coefficients that were just 1% of the apparent cosmogenic ^{3}He coefficients in their quartz sample.

Argunova et al. (2003) recently reported a helium diffusion coefficient of $~2.5 \times 10^{-8}$ cm^2/s at 250°C in synthetic and possibly fluid inclusion bearing quartz crystals with a dislocation density of 10^2/cm^2. For reference, the parameters of Trull et al. (1991) predict a diffusivity that is nearly 3 orders of magnitude lower at that temperature, and the parameters reported here predict a value 20 times higher. The results of Argunova et al. (2003) also suggest that an increase in dislocation density results in a substantial increase in the diffusion coefficient and decrease in activation energy. The effects of dislocation assisted diffusion were investigated by Klyavin (1993) who concluded that the transport of helium atoms to the surface layers of LiF crystals is clearly accelerated by the movement of dislocations. The results of Argunova et al. (2003) suggest that a similar effect of dislocation assisted helium diffusion also occurs in quartz. Although we did not estimate the dislocation density of our sample, significant differences in defect density between our sample and previously analyzed quartz samples may also influence the discrepancy between reported helium diffusion parameters.

4.5. Implications for Cosmogenic Nuclide Retentivity

Because quartz samples used for cosmogenic nuclide investigations may contain fluid and mineral inclusions, the diffusion kinetics of our study may not directly apply in certain cases. Instead, our results likely represent an end-member case of purely solid-state diffusion within the quartz lattice. The presence of isolated fluid inclusions, even if very small, would have a net effect of increasing noble gas retentivity. Aside from the potential additional effect of radiation damage which may also enhance noble gas retentivity (discussed above; see section 4.3), the parameters summarized in Table 3 describe the diffusion kinetics which control neon and helium mobility between fluid inclusions and possibly defects in a crystal.

Therefore, assuming that the three proton-induced nuclides are analogous to cosmogenic isotopes of neon and helium, their diffusion kinetics indicates that quartz will retain neon much

Table 4. Stepped heating results (Experiment 2, lower proton dose).[a]

Step	T (°C)	t (h)	³He (×10⁶ atoms)	± (×10⁶ atoms)	²¹Ne	±
1	99.6	0.25	4.30	0.38	—	—
2	99.8	0.50	5.87	0.37	—	—
3	99.9	1.00	8.09	0.44	—	—
4	79.9	1.00	1.56	0.19	—	—
5	79.9	1.00	1.44	0.19	—	—
6	69.9	2.00	0.84	0.41	—	—
7	70.0	2.00	1.19	0.21	—	—
8	89.9	1.00	2.25	0.03	—	—
9	89.9	1.50	2.97	0.26	—	—
10	99.9	1.50	4.97	0.26	—	—
11	119.8	0.50	4.97	0.37	—	—
12	119.8	0.50	3.55	0.35	—	—
13	119.8	0.50	2.89	0.26	—	—
14	139.8	0.50	7.28	0.26	—	—
15	139.8	0.50	4.80	0.39	—	—
16	139.9	1.00	6.24	0.37	—	—
17	159.7	0.50	8.60	0.41	—	—
18	159.9	1.00	10.81	0.47	—	—
19	174.8	0.50	7.34	0.65	0.11	0.06
20	174.8	0.50	5.45	0.52	0.03	0.06
21	199.9	1.00	14.61	0.38	0.43	0.08
22	199.8	0.50	2.15	0.59	0.14	0.07
23	224.9	0.50	2.22	0.25	0.59	0.09
24	224.9	1.00	0.57	0.26	0.60	0.09
25	249.9	0.50	0.06	0.03	1.03	0.12
26	250.0	1.00	0.02	0.03	1.40	0.14
27	275.0	0.50	—	—	2.35	0.17
28	275.0	1.00	—	—	2.83	0.18
29	299.9	0.50	—	—	3.90	0.21
30	299.9	1.00	—	—	5.30	0.20
31	324.9	0.50	—	—	6.74	0.23
32	325.0	1.00	—	—	8.59	0.32
33	349.9	0.50	—	—	9.33	0.32
34	349.9	1.00	—	—	10.17	0.37
35	337.9	1.00	—	—	3.41	0.23
36	312.9	1.25	—	—	0.95	0.13
37	287.9	1.50	—	—	0.27	0.07
38	262.0	2.00	—	—	0.11	0.06
39	250.0	2.00	—	—	0.04	0.04
40	275.0	1.50	—	—	0.17	0.05
41	299.9	1.00	—	—	0.37	0.06
42	324.8	0.50	—	—	0.64	0.08
43	349.9	1.00	—	—	3.57	0.10
44	374.9	1.00	—	—	5.34	0.19
45	399.9	1.00	—	—	4.65	0.30
46	424.9	1.00	—	—	4.16	0.21
Fusion	~1300	0.5	—	—	10.25	0.00
Total			115.1		87.5	

[a] All values are corrected for blank contributions. A dash indicates below detection limit. Mass analyzed = 2.80 mg.

more effectively than helium in nature. Extrapolating the diffusion parameters in Table 2 to 20°C predicts that a typically sized quartz grain would not retain significant cosmogenic ³He over geologic time, whereas cosmogenic ²¹Ne would be quantitatively retained. For example, assuming the analyzed grain size equals the diffusion domain size, we estimate diffusion coefficients of 6 $(^{+9}/_{-4})$ × 10^{-24} cm²/s and 1 $(^{+1.3}/_{-0.6})$ × 10^{-13} cm²/s for ²¹Ne and ³He, respectively, at 20°C. These diffusivities predict that a 100 μm quartz grain (here and below dimensions are radii) will retain ~97% of in situ produced ²¹Ne over 100 Myr of production at 20°C. A 1 mm grain would lose only 1% of its in situ produced ²¹Ne over 100 Myr at a mean temperature of 30°C.

Figure 4 shows ²¹Ne retentivity as a function of temperature and grain size. Curves indicate the conditions under which 5% ²¹Ne loss will occur for four different exposure durations. Although in many conditions quartz is highly retentive, the figure shows that neon may be lost from even fairly large grains (mm size) at temperatures only slightly higher than ambient earth surface conditions. For example, samples exposed to solar heating in un-vegetated terrain are likely to have experienced such conditions.

An additional consideration for ²¹Ne exposure dating is the presence of nucleogenic neon from decay of U and Th series nuclides. Samples that have low nucleogenic ²¹Ne concentrations yield by far the most reliable exposure ages (Phillips et
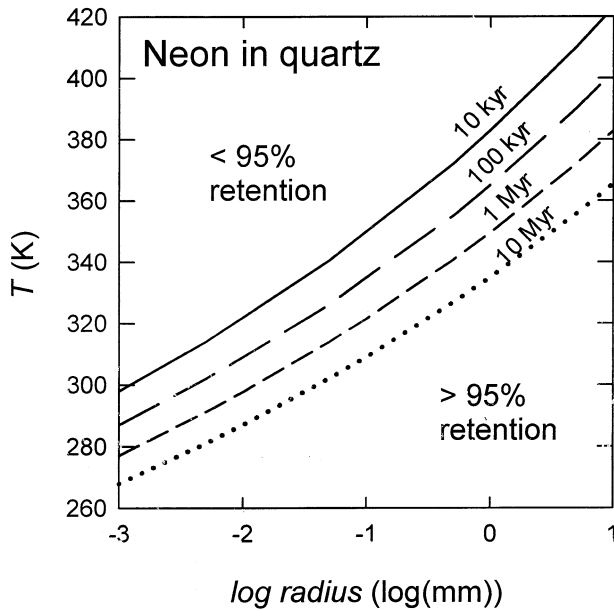
Fig. 4. Neon retentivity in quartz. Shown are the threshold temperatures at which 5% diffusive loss would occur in quartz as a function of grain radius for four different isothermal accumulation times (indicated on curves). The calculation is based on the accumulation-diffusion equation as described in Wolf et al. (1998) but modified for cosmogenic production of ^{21}Ne in quartz and uses the proton-induced ^{21}Ne diffusion kinetics in Table 2. The calculation is for a spherical diffusion domain and assumed zero concentration boundary condition.

al., 1998). Our data indicate that a 500 μm quartz grain has a ^{21}Ne closure temperature of 94 ± 6°C (10°C/Myr cooling rate). Thus, in the absence of fluid inclusions, quartz samples recently exhumed from temperatures in excess of this value will likely have low nucleogenic ^{21}Ne concentrations, while those that have remained below this temperature for geologically log periods will likely have very high nucleogenic ^{21}Ne concentrations.

The helium diffusion parameters predict that only large quartz grains will retain any significant amount of cosmogenic ^{3}He at all. A 5 mm grain would rapidly reach a steady-state exposure age of ~3500 yr after only 25,000 yr of accumulation at 20°C. At near Earth surface temperatures, inclusion free quartz is effectively wide open to diffusive helium loss, yet completely closed to neon.

4.6. Physical Implications

Of particular relevance to understanding solid state diffusion is the substantial difference between the diffusion kinetics of neon and helium. The physics which results in the many orders of magnitude difference between the diffusivity of neon and helium is not immediately obvious. Despite a wide range in estimated van der Waals radii for the noble gases (0.93–1.48 Å and 1.12–1.58 Å for helium and neon, respectively; Badenhoop and Weinhold, 1997), all estimates predict a small size difference (mean difference ~ 13%) relative to the mass difference between the two elements. Classical transition state theories of solid state diffusion predict that the frequency factors, D_o, of two diffusing isotopes should vary as the inverse square root of

their masses or reduced masses (Shelby, 1971). Due to their common inert chemical behavior, if we ignore their size difference and consider ^{21}Ne and ^{3}He to be two "isotopes" of one another, the inverse root mass relationship predicts that ^{3}He diffusivity should exceed ^{21}Ne diffusivity by only a factor of ~2.6. And, if ^{21}Ne and ^{3}He behave as two isotopes only differing in mass, the classical theories would also predict the E_a of each to be approximately equal. These relationships are clearly not observed.

Although small, the difference between the atomic size of helium and neon must have a profound effect upon their respective rates of diffusion. Quartz has elongated channels along the z-axis likely to act as diffusive pathways with an effective diameter equal to 2.4–2.6 Å (Kalashnikov et al., 2003). This is very near to the atomic diameter of both helium and neon. Using ab initio calculations, Kalashnikov et al. (2003) predicted the activation energy of helium migration through the quartz crystalline lattice by considering the interaction between the helium atom and the neighboring constituents of the channel wall (primarily the Si atoms; (Kalashnikov et al., 2003). The calculated activation energy is a function of the shear modulus for the SiO$_2$ channels and the polarizability of helium in a given quantum state. They conclude that the diffusion kinetics of helium in quartz is orders of magnitude slower than in amorphous SiO$_2$ because of the displacements imparted upon the channel wall atoms by the migrating helium atom. Kalashnikov et al. (2003) conclude that only a metastable helium atom in the triplet state (2 ^{3}S$_1$) can penetrate through the channel, with a calculated activation energy ~29 kJ/mol. Although their calculation demonstrates the influence that atomic size has upon helium diffusion in quartz, the discrepancy between our observed and their calculated activation energies is not currently understood.

If the results of Kalashnikov et al. (2003) indicate that the diffusivity of helium is strongly affected by the size of the diffusive channel, then it is conceivable that a size threshold may exist between the diameters of helium and neon which could significantly affect their relative diffusivities in quartz. The apparent activation energy difference between neon and helium diffusivity (69 ± 1 kJ/mol) may represent the energy barrier associated with this effect. Although the propagated uncertainty in ab initio calculations may be prohibitively large to test this hypothesis, the experimentally observed difference between neon and helium diffusion kinetics provides constraints which may be used to test size and quantum effect hypotheses.

Shelby (1971) called upon quantum effects to explain a temperature dependence of the helium isotope diffusivity ratio observed in vitreous silica. Classical transition state theory and the quantum effect described by Shelby (1971) predict small isotope effects, which are not observed in the helium results presented here. To within analytical uncertainties, we find for the proton-induced isotopes a conservatively constrained ratio D^{4}He/D^{3}He = 1.00 ± 0.05 (Fig. 2). That we find no significant difference between the diffusivity of proton-induced ^{3}He and ^{4}He suggests that neither the classical nor the quantum transition state theory completely explains the mobility of helium through the quartz lattice. It is of interest that the diffusive fractionation of helium and neon isotopes has so far been experimentally observed in nonordered solids (Frank et al.,

1961; Shelby, 1971; Trull and Kurz, 1999) yet not observed here or in other natural crystalline solids (Shuster et al., 2004). As suggested by Shuster et al. (2004), the lack of a helium isotope effect implies that the mobility of at least proton-induced helium may be controlled by a process that is more complicated than simple volume diffusion such as dislocation assisted or enhanced diffusion (Klyavin, 1993; Shuster et al., 2004). If so, the same phenomenon does not appear to control the diffusivity of proton-induced neon in quartz. By the time in the experiment when the helium had become totally exhausted from the sample, only 1% of the neon had been removed. If defect mobility had enhanced the diffusion of helium during the experiment, the same defect mobility could have at most had a negligible affected upon the neon mobility.

5. CONCLUSIONS

These experimental results confirm empiric observations that quartz can quantitatively retain neon over geologic time at Earth surface temperatures, yet rapidly diffuse helium. Although quartz is highly retentive to neon, the affects of grain size and elevated temperatures due to solar heating need to be considered when interpreting ^{21}Ne concentrations, in particular for grains smaller than ~ 1 mm collected from arid, mid-, and low-latitude localities. The difference in the activation energy for neon and helium diffusion is $\sim$70 kJ/mol. This energy provides a fundamental constraint with which to test theories of solid state diffusion, and likely reflects the effect of size upon noble gas diffusion in quartz. This experiment demonstrates the utility that inducing single component, purely synthetic noble gases within minerals via proton bombardment has for the study of solid state noble gas diffusion.

REFERENCES

Argunova T. S., Sorokin L. M., Pevzner B. Z., Balitskii V. S., Gannibal M. A., Je J. H., Hwu Y., and Tsai W. L. (2003) The influence of defects in the crystal structure on helium diffusion in quartz. *Phys. Solid State* **45** (*10*), 1910–1917.

Badenhoop J. K. and Weinhold F. (1997) Natural steric analysis: Ab initio van der Waals radii of atoms and ions. *J. Chem. Phys.* **107** (*14*), 5422–5432.

Brook E. J. and Kurz M. D. (1993) Surface-exposure chronology using in situ cosmogenic He-3 in Antarctic quartz sandstone boulders. *Quat. Res.* **39** (*1*), 1–10.

Bruno L. A., Baur H., Graf T., Schluchter C., Signer P., and Wieler R. (1997) Dating of Sirius Group tillites in the Antarctic dry valleys with cosmogenic He-3 and Ne-21. *Earth Planet. Sci. Lett.* **147** (*1–4*), 37–54.

Cerling T. and Craig H. (1993) Geomorphology and in-situ cosmogenic isotopes. *Ann. Rev. Earth Planet. Sci.* **22,** 273–317.

Cerling T. E., Poreda R. J., and Rathburn S. L. (1994) Cosmogenic He-3 and Ne-21 age of the Big Lost River Flood, Snake River Plain, Idaho. *Geology* **22** (*3*), 227–230.

Crank J. (1975) *The Mathematics of Diffusion.* Oxford University Press.

Dunai T. and Roselieb K. (1996) Sorption and diffusion of helium in garnet: Implications for volatile tracing and dating. *Earth Planet. Sci. Lett.* **139,** 411–421.

Farley K. A. (2000) Helium diffusion from apatite: General behavior as illustrated by Durango fluorapatite. *J. Geophys. Res.* **105,** 2903–2914.

Farley K. A., Reiners P. W., and Nenow V. (1999) An apparatus for high-precision helium diffusion measurements from minerals. *Anal. Chem.* **71,** 2059–2061.

Fechtig H. and Kalbitzer S. (1966) The diffusion of argon in potassium bearing solids. In *Potassium-Argon Dating* (eds. O. A. Schaeffer and J. Zahringer), pp. 68–106. Springer.

Frank R. C., Lee R. W., and Swets D. E. (1961) Diffusion of neon isotopes in fused quartz. *J. Chem. Phys.* **35** (*4*), 1451–1459.

Friedlander G., Kennedy J. W., Macias E. S., and Miller J. M. (1981) *Nuclear and Radiochemistry.* Wiley.

Funk H., Baur H., Frick U., Schultz L., and Signer P. (1971) Diffusion of helium in quartz. *Zeitsch. Kristallogr. Kristallgeo. Kristallphys. Kristallchem.* **133,** 225–233.

Graf T., Kohl C. P., Marti K., and Nishiizumi K. (1991) Cosmic ray–produced neon in Antarctic rocks. *Geophys. Res. Lett.* **18** (*2*), 203–206.

Hetzel R., Niedermann S., Ivy-Ochs S., Kubik P. W., Tao M. X., and Gao B. (2002) Ne-21 versus Be-10 and Al-26 exposure ages of fluvial terraces: The influence of crustal Ne in quartz. *Earth Planet. Sci. Lett.* **201** (*3–4*), 575–591.

Horn P., Jessberger E. K., Kirsten T., and Richter H. (1975) ^{39}Ar-^{40}Ar dating of lunar rocks: Effects of grain size and neutron irradiation. *Geochim. Cosmochim. Acta* (Suppl. 6), 1563–1591.

Kalashnikov E., Tolstikhin I., Lehmann B., and Pevzner B. (2003) Helium transport along lattice channels in crystalline quartz. *J. Phys. Chem. Solids* **64** (*11*), 2293–2300.

Klyavin O. V. (1993) Dislocation-dynamic diffusion in crystalline bodies. *Phys. Solid State* **35** (*3*), 261–277.

Lal D. (1988) In situ–produced cosmogenic isotopes in terrestrial rocks. *Annu. Rev. Earth Planet. Sci.* **16,** 355–388.

Leya I., Busemann H., Baur H., Wieler R., Gloris M., Neumann S., Michel R., Sudbrock F., and Herpers U. (1998) Cross sections for the proton-induced production of He and Ne isotopes from magnesium, aluminum and silicon. *Nucl. Instr. Methods Phys. Res. B* **145,** 449–458.

Leya I., Lange H. J., Neumann S., Wieler R., and Michel R. (2000) The production of cosmogenic nuclides in stony meteoroids by galactic cosmic-ray particles. *Meteor. Planet. Sci.* **35** (*2*), 259–286.

Libarkin J. C., Quade J., Chase C. G., Poths J., and McIntosh W. (2002) Measurement of ancient cosmogenic Ne-21 in quartz from the 28 Ma Fish Canyon Tuff, Colorado. *Chem. Geol.* **186** (*3–4*), 199–213.

Lovera O., Richter F., and Harrison T. (1989) The ^{40}Ar/^{39}Ar thermochronometry for slowly cooled samples having a distribution of diffusion domain sizes. *J. Geophys. Res.* **94,** 17917–17935.

Luther L. C. and Moore W. J. (1964) Diffusion of helium in silicon germanium + diamond. *J. Chem. Phys.* **41** (*4*), 1018–1026.

Masarik J., Frank M., Schafer J. M., and Wieler R. (2001a) Correction of in situ cosmogenic nuclide production rates for geomagnetic field intensity variations during the past 800,000 years. *Geochim. Cosmochim. Acta* **65** (*17*), 2995–3003.

Masarik J., Nishiizumi K., and Reedy R. C. (2001b) Production rates of cosmogenic helium-3, neon-21 and neon-22 in ordinary chondrites and the lunar surface. *Meteor. Planet. Sci.* **36** (*5*), 643–650.

McDougall I. and Harrison T. M. (1999) *Geochronology and Thermochronology by the ^{40}Ar/^{39}Ar Method.* Oxford University Press.

Niedermann S. (2002) Cosmic-ray-produced noble gases in terrestrial rocks: Dating tools for surface processes. In *Noble Gases in Geochemistry and Cosmochemistry,* Vol. 47 (ed. D. Porcelli, C. J. Ballentine, and R. Wieler), pp. 731–777.

Niedermann S., Graf T., and Marti K. (1993) Mass spectrometric identification of cosmic-ray produced neon in terrestrial rocks with multiple meom components. *Earth Planet. Sci. Lett.* **118,** 65–73.

Onstott T. C., Miller M. L., Ewing R. C., Arnold G. W., and Walsh D. S. (1995) Recoil refinements—Implications for the Ar-40/Ar-39 dating technique. *Geochim. Cosmochim. Acta* **59** (*9*), 1821–1834.

Phillips W. M., McDonald E. V., Reneau S. L., and Poths J. (1998) Dating soils and alluvium with cosmogenic Ne-21 depth profiles: Case studies from the Pajarito Plateau, New Mexico, USA. *Earth Planet. Sci. Lett.* **160** (*1–2*), 209–223.

Schafer J. M., Ivy-Ochs S., Wieler R., Leya J., Baur H., Denton G. H., and Schluchter C. (1999) Cosmogenic noble gas studies in the oldest landscape on earth: Surface exposure ages of the Dry Valleys, Antarctica. *Earth Planet. Sci. Lett.* **167** (*3–4*), 215–226.

Shelby J. E. (1971) Diffusion of helium isotopes in vitreous silica. *Phys. Rev. B* **4** (*8*), 2681–2686.

Shuster D. L. and Farley K. A. (2004) ^{3}He/^{4}He thermochronometry. *Earth Planet. Sci. Lett.* **217** (*1–2*), 1–17.

Shuster D. L., Farley K. A., Sisterson J. M., and Burnett D. S. (2004) Quantifying the diffusion kinetics and spatial distributions of radiogenic ^{4}He in minerals containing proton-induced ^{3}He. *Earth Planet. Sci. Lett.* **217** (*1–2*), 19–32.

Shuster D. L., Vasconcelos P. M., Heim J. A., and Farley K. A. (2005) Weathering geochronology by (U-Th)/He dating of goethite. *Geochim. Cosmochim. Acta* **69** (*3*), 659–673.

Trull T. W., Kurz M. D., and Jenkins W. J. (1991) Diffusion of cosmogenic 3He in olivine and quartz: Implications for surface exposure dating. *Earth Planet. Sci. Lett.* **103,** 241–256.

Trull T. W., Brown E. T., Marty B., Raisbeck G. M., and Yiou F. (1995) Cosmogenic Be-10 and He-3 accumulation in Pleistocene beach terraces in Death Valley, California, USA—Implications for cosmic-ray exposure dating of young surfaces in hot climates. *Chem. Geol.* **119** (*1–4*), 191–207.

Trull T. W. and Kurz M. D. (1999) Isotopic fractionation accompanying helium diffusion in basaltic glass. *J. Mol. Structure* **485,** 555–567.

Watson E. B. and Cherniak D. J. (2003) Lattice diffusion of Ar in quartz, with constraints on Ar solubility and evidence of nanopores. *Geochim. Cosmochim. Acta* **67** (*11*), 2043–2062.

Wieler R. (2002) Cosmic ray–produced noble gases in meteorites. In *Noble Gases in Geochemistry and Cosmochemistry,* Vol. 47 (ed. D. Porcelli, C. J. Ballentine, and R. Wieler), pp. 125–163.

Wiens R. C., Lal D., Rison W., and Wacker J. F. (1994) Helium isotope diffusion in natural diamonds. *Geochim. Cosmochim. Acta* **58** (*7*), 1747–1757.

Wolf R. A., Farley K. A., and Kass D. M. (1998) A sensitivity analysis of the apatite (U-Th)/He thermochronometer. *Chemical Geology* **148**, 105–114.